Eur. Phys. J. D **40**, 125–132 (2006)
DOI: 10.1140/epjd/e2006-00154-7

THE EUROPEAN PHYSICAL JOURNAL D

Longitudinal coherence and spectral profile of a nickel-like silver transient soft X-ray laser

O. Guilbaud[1,a], A. Klisnick[1], D. Joyeux[2], D. Benredjem[1], K. Cassou[1], S. Kazamias[1], D. Ros[1], D. Phalippou[2], G. Jamelot[1], and C. Möller[1]

[1] LIXAM, Université Paris Sud, Campus d'Orsay, bâtiment 350, 91405 Orsay Cedex, France
[2] LCFIO, Institut d'Optique, Campus d'Orsay, bâtiment 503, 91403 Orsay Cedex, France

Received 15 December 2005 / Received in final form 16 March 2006
Published online 30 June 2006

Abstract. The spectral width of a Ni-like silver transient soft X-ray laser ($4d$-$4p$ $\lambda = 13.9$ nm) was experimentally inferred from the measurement of its temporal coherence, performed with a novel wavefront division interferometer. The measured coherence time of 3 ps corresponds to a spectral linewidth of 0.7 mÅ which is narrow. We compare this experimental result to numerical simulations of the amplified line profile, performed along two different approaches. Both calculations predict a spectral linewidth that is about 3 times larger than the experimental value. We discuss several effects that might explain this discrepancy. We show that, due to the short duration of the X-ray laser pulse, the assumption of a stationary electromagnetic field used in both the experimental analysis and in the calculations need to be reconsidered.

PACS. 42.55.Vc X- and gamma-ray lasers – 52.50.Jm Plasma production and heating by laser beams (laser-foil, laser-cluster, etc.) – 32.30.Rj X-ray spectra

1 Introduction

Soft X-ray lasers are high brightness sources emitting short wavelength radiation from 30 nm to 3 nm [1]. Their amplifying media is a hot, dense and highly charged plasma rod containing a large fraction of closed shell lasing ions (neon-like, nickel-like or palladium-like ions). This plasma is generated by the interaction of an intense infrared laser pulse with a target [2] or by a high intensity capillary discharge in a rare gas [3]. Until now, in all the soft X-ray lasers operating at saturation, the population inversion between the levels of the lasing ions is induced by electron collisional excitations, leading to high gain value at short wavelength. The short lifetime of the gain and the absence of high reflectivity X-UV optics, make the use of this X-UV amplifier in a complete optical cavity impossible. For this reason, the soft X-ray laser emission results from the single-pass amplification of the ion spontaneous emission. Because of the high gain values, saturation regime can be achieved and high intensity is obtained. Due to the narrow intrinsic ion linewidth and to the gain narrowing, the soft X-ray lasers are the most monochromatic sources in this wavelength range.

Recently, important progress has been achieved by the development of transient collisionnal excitation (TCE) soft X-ray laser in which the creation of plasma with lasing ions and the pumping of population inversions are achieved in two separate steps [4]. First, a nanosecond background infrared laser pulse creates the plasma in the appropriate ionisation stage. Then a short (picosecond) compressed pulse heats the free electrons of the plasma to temperatures higher than 500 eV inducing the collisionnal pumping and producing the laser gain. This scheme leads to a dramatic decrease of the required laser pumping energy. More recently optimisation of the coupling of the short pulse with the preformed plasma led to high repetition rate saturated soft X-ray lasers with compact Ti:sapphire laser facilities [5,6].

TCE soft X-ray lasers have a gain lifetime of the order of 10 to 30 ps. This characteristic has important consequences both on practical and fundamental levels. First, the gain lifetime is shorter than the travelling time of the amplified photon along the plasma rod [7]. Travelling wave (TW) pumping is implemented to achieve constant amplification of the soft X-ray during its propagation [8]. Second, the TCE soft X-ray laser emits brief picosecond X-UV pulses. Pulse durations shorter than 6 ps have been demonstrated [9,10]. Moreover, the moderate temperature of the lasing ion is expected to lead to a very narrow soft X-ray spectral line and hence to a high longitudinal coherence, with a coherence time of the order of the soft X-ray laser pulse duration. However, because of the narrow linewidth, only few experiments have so far been performed to measure it, most of them relying on Fourier-Transform spectroscopy principles.

[a] e-mail: o_guilbaud@yahoo.fr

In a previous paper [11], we reported experimental investigations of the longitudinal coherence of a Ni-like silver TCE soft X-ray laser, emitting at the wavelength $\lambda = 13.9$ nm ($4d \rightarrow 4p, J = 0 \rightarrow 1$ transition). Measurement of the longitudinal coherence has been performed with a new X-UV achromatic and versatile wavefront-division interferometer. The design of this interferometer avoids the use of X-UV beam splitters so that it can be used on a large wavelength range with low wavefront degradation. A longitudinal coherence length of 850 μm has been reported, three times longer than the value previously reported by Smith et al. [12] on a Ni-like Pd soft X-ray laser ($\lambda = 14.7$ nm). In order to explain the origin of this high value, we present in this paper, a study of the spectral line shape and width of the soft X-ray laser line. Numerical simulations were performed to understand these experimental results. Details of these models and comparisons with experiments are given. The mechanisms that might be involved in the generation of a high longitudinal coherence are finally discussed.

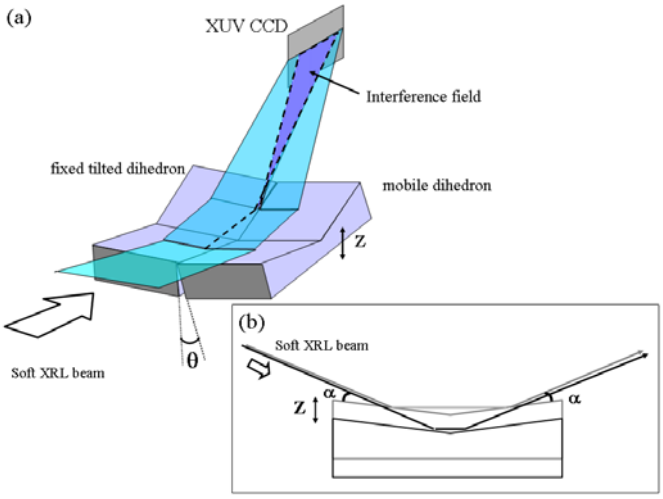

Fig. 1. (a) Schematic overview of the XUV interferometer used for longitudinal coherence measurement. The optical interfering elements consist of a pair of grazing incidence dihedrons, slightly tilted towards each other. (b) One of the dihedrons can be translated vertically (z) to introduce a controlled path difference between the two X-ray laser interfering half-beams, without changing the geometry of their transverse superposition.

2 Measurement of temporal coherence and spectral profile

In this section, we will show how the spectral profile of the 13.9 nm laser line was deduced from the experimental measurement of the temporal coherence. We will first briefly recall the conditions of the experiments in which high quality X-UV interferograms were recorded. The variation of fringe visibility as a function of the path difference between the interfering X-ray laser beams was used to infer the temporal coherence length, as described in [11]. Here we will discuss further the analysis of the experimental data, in particular with respect to the existence of fluctuations of the fringe visibility within a single-shot interferogram and from shot to shot.

The Ni-like Ag transient soft X-ray laser was generated with the 100 TW CPA Nd-Glass laser chain ($\lambda_{IR} = 1054$ nm) of the LULI facility. More details on this experimental setup can be found in [11]. The lasing plasma is produced by a 600 ps background laser pulse focused on a 10 mm long solid silver slab target. The laser beam is focused along a 23 mm $\times$ 200 μm focal line by the combination of cylindrical and spherical lenses. A short compressed (0.4 ps) pulse interacts with the plasma 250 ps after the background pulse intensity peak. The short pulse is focused along a 20 mm $\times$ 80 μm focal line by the combination of a parabolic and a spherical mirror [13]. This pumping configuration was previously shown to improve the spatial uniformity of the X-ray laser emitting aperture [14]. The energy of the background pulse on the target surface was 12 J/cm, corresponding to an irradiance of $\sim 10^{12}$ Wcm^{-2},while the short heating pulse carried a 5 J/cm energy and irradiated the target with an irradiance of $\sim 10^{15}$ Wcm^{-2}. The travelling wave (TW) irradiation at a speed $v = c$ was implemented on the short pulse beam. Prior to the longitudinal coherence measurement described below, the X-ray laser beam was first monitored with a X-UV beam far-field imaging system. The uniformity, divergence, and deflection angle of the beam were characterized. The dimensions, energy and uniformity of the emitting aperture were also measured with a X-UV near-field imaging system, consisting of an X-UV ellipsoidal mirror coated with Mo-Si multilayers [14,15]. This device imaged the output plane of the amplifying plasma on an X-UV CCD camera, with high spatial resolution (1 μm).

The X-ray laser beam was finally directed toward a wavefront division interferometer specifically designed for measuring the temporal coherence. This diagnostic was placed at a distance of 3.5 m from the source, in order to ensure a significant transverse coherence length of the beam at the entrance of the interferometer. A complete description of this interferometer can be found in [11]. This device is composed of a pair of bare silica roof-shaped mirrors, or dihedrons, which are placed side by side and are slightly tilted towards each other transversally to the general direction of the beam. The X-ray laser beam is directed to the dihedron pair, with its incidence axis along their common edge and with a 6° grazing incidence angle. Because the two dihedrons are tilted, the incident beam is reflected into two separated half-beams that slightly converge towards each other and overlap. The fringes that are formed in the overlapping region are detected onto an XUV CCD (10^6 pixels, 16 bits, Andor Technology) which is placed at 50 cm from the dihedrons, and tilted at angle of 9° from the incident beam in order to increase the apparent fringe spacing (see Fig. 1). The path difference ℓ between the two interfering half-beams was varied from shot to shot by accurately translating one of the two dihedrons vertically. Dihedrons were used rather than simple

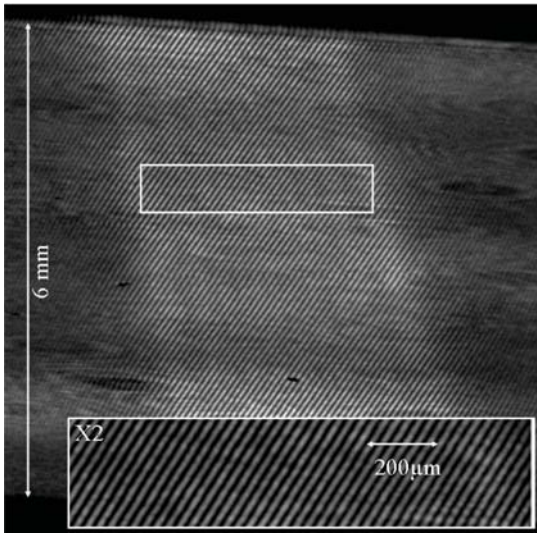

Fig. 2. Interferogram obtained with the 13.9 nm TCE X-ray laser for a path difference set to zero. The horizontal scale is not corrected from the anamorphosis caused by the CCD inclination. The fringe visibility is close to 50%. A large-scale, spatial modulation of the average intensity of the interference fringes is apparent.

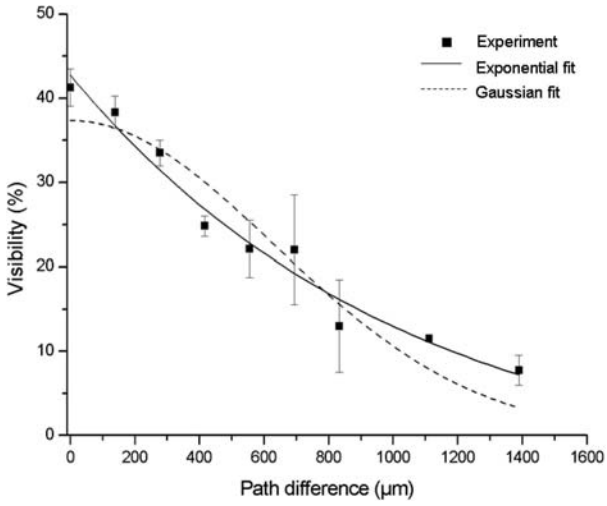

Fig. 3. Variation of the measured fringe visibility versus path difference ℓ. Black squares represent the shot-averaged value of the measured fringe visibility for a given path difference. The vertical bars give the standard deviation. Two different usual analytical functions were used to fit the data: a decreasing exponential and a Gaussian function (see text and Tab. 1).

flat mirrors to ensure that the conditions of spatial coherence are kept constant while changing the path difference. The zero path difference of the system (i.e. when the two dihedrons are exactly at the same height) was determined before the experiment, with a very good accuracy (1 μm or 100λ) by determining the zero order interference fringe with an optical white source (Hg spectral lamp).

Figure 2 presents a typical interferogram, obtained with a path difference set to zero. The interference field in the detection plane is 6 mm in the vertical direction and 510 μm in the horizontal one. The insert shows a local magnification of the interferogram. The actual fringe spacing is 12 μm, and the interferogram exhibits large scale modulation of the signal within the recorded field. This modulation of the interferogram is attributed to the existence of intensity non-uniformities in the X-ray laser incident beam which were observed to have similar spatial scales. The numerical treatment of the interferograms consisted in a background substraction performed from data taken outside the beam field, followed by a Fourier transform processing performed in a small sliding window. This yields the map of local fringe visibility $V(\ell)$ over the interference field. The fringe visibility was found to vary by several 10% across the interference field. This spatial variation was attributed mainly to the above mentioned non-uniformities in the X-ray laser beam. This eventually leads to unbalanced time-averaged intensities I_1 and I_2 in the two interfering half-beams and to a local reduction of the fringe visibility. In the analysis of our interfometric data we have thus made the two following important assumptions: (i) the spatial and longitudinal coherence of the X-ray laser beam is constant within the small part (6 mm $\times$ 0.5 mm) of the whole beam section (20 mm $\times$ 60 mm) sampled by the dihedron pair; (ii) the relevant value of fringe visibility in each interferogram is the maximum one, which is the best estimation of the visibility that would be produced by equal intensity interfering beams ($I_1 = I_2$).

Figure 3 shows the graph of the measured fringe visibility $V(\ell)$ as a function of the path difference. Several shots were performed for each value of the path difference, at fixed irradiation conditions. The black squares plotted in Figure 3 are the shot-averaged value V of the measured visibilities for each path difference ℓ. The visibility is strongly reduced while increasing the path difference from 0 mm to 1.39 mm (or $10^5\lambda$). However, even for the larger values of ℓ, the fringe pattern was still clearly visible and the signal to noise ratio high enough to allow an accurate quantitative measurement of the fringe visibility. Shot to shot fluctuations of the visibility were observed, with a maximum relative amplitude of 30%. The vertical bars shown in Figure 3 give the visibility standard deviation.

The fringe visibility for $\ell = 0$ μm is smaller than 1. We show that this is consistent with a partially spatially coherent source. The spatial coherence of transient X-ray lasers at their output plane is shown to be small [16]. The mutual coherence between the two half-beams at the entrance of the interferometer can be estimated, with the Van Cittert Zernicke theorem [17], assuming that the X-ray laser exit aperture is a spatially incoherent source with a finite size. The near-field images obtained during the experiment showed that the average source intensity distribution at the exit of the plasma can be modelled by a Gaussian profile distribution in both vertical and horizontal directions with average full width at half maximum of respectively 100 μm and 40 μm. This model yields a fringe visibility of 55%, for $\ell = 0$ μm at 3.5 m from the source, consistent with the measured value. Besides, this

Table 1. Results of the fringe visibility evolution fit by a decreasing exponential and a Gaussian function.

$V(\ell)$	ℓ_C (μm)	χ^2_R	$\Delta\lambda$ (mÅ)
exponential	840 ± 70	0.87	0.73 ± 0.06
Gaussian	890 ± 75	4.57	1.15 ± 0.10

calculation also helps explain the shot-to-shot fluctuation of the fringe visibility for a fixed path difference, as being due to shot-to-shot variations of the X-ray laser source horizontal width and shape. Such variations were indeed observed by the near-field imaging diagnostic in our experiment. The horizontal size of the source was found to be of 40 μm in average but did vary from 30 μm to 50 μm from shot-to-shot. We have checked that such variations lead to a relative fluctuation of the fringe visibility of 30% for any path difference, in agreement with the observed scattering of the experimental data.

The experimental data were fitted with a Gaussian and an exponentially decreasing function, which are also shown in Figure 3. Results of the fits are presented in Table 1. We find that a Gaussian fit is not consistent with the experimental data, which are more adequately described by an exponential decrease, specially for great ℓ values. This is quantitatively shown by the reduced chi-squared χ^2_R: $\chi^2_R = 4.57$ for the Gaussian case and $\chi^2_R = 0.87$ for the exponential case. However, Table 1 shows that both fits lead to comparable values of the coherence length, which is defined as the path difference that decreases the maximal visibility by a factor $1/e$: $\ell_C = 850 \pm 75$ μm. This is to our knowledge the largest longitudinal coherence length ever measured for a soft X-ray laser source. It corresponds to a coherence time of $\tau_C = 2.8 \pm 0.3$ ps. These values can be compared to the results obtained by Smith et al. [12] who have measured the longitudinal coherence of a Pd-like transient soft X-ray laser ($\lambda = 14.7$ nm) using a XUV Michelson interferometer. The authors found a Gaussian evolution of the fringe visibility with the path difference. Furthermore, the coherence length was found to be two to three times smaller ($\ell_C = 350$ μm).

These results hence contrast with our observations. One possible explanation for this apparent disagreement could lie in the fact that our measurements extend to larger values of the path difference (up to $\ell = 1400$ μm) where the visibility is low. By contrast in Smith et al. the measurement is limited to $\ell = 700$ μm where the measured visibility is zero, but the authors point out that values of visibility below 20% were difficult to quantify. This could thus have led to an underestimation of the inferred coherence length.

The fringe visibility is proportional to the modulus of the complex degree of longitudinal coherence $\gamma(\tau) = \gamma(\ell/c)$. Using the Wiener-Khintchine theorem, which states that the spectral line profile $\rho(\nu)$ is the Fourier transform of the longitudinal degree of coherence, the spectral width and profile of the laser line can be deduced from the experimental curve represented in Figure 3. Then, considering the exponential shape of the fringe visibility evolution, we find that the X-ray laser line has a Lorentzian spectral profile. The linewidth $\Delta\nu$ (FWHM) and the coherence length are inversely related. For the Lorentzian profile the linewidth is $\Delta\nu = 1.13 \pm 0.08 \times 10^{11}$ Hz or $\Delta\lambda = 0.73 \pm 0.06$ mÅ. Table 1 shows that a linewidth approximately 1.6 times larger would be inferred from the Gaussian fit. Compared to these values, Smith et al. [12] found a Gaussian spectral line profile with a width four time larger than in our experiment.

3 Modelling of the soft X-ray laser line profile

In this section, we present numerical calculations of the X-ray laser line profile in our experimental conditions. The modelling of the line profile involves the description of the optically-thin profile modified through amplification along the active plasma. The line profile is determined by ion level properties and by local plasma conditions, such as ion temperature T_i, spontaneous emission power density σ, small-signal gain G_{SS} and saturation intensity I_{sat}. A code describing both plasma hydrodynamics, ion and level populations has been used to model this aspect. The effect of amplification on the final output line profile was modelled following two different approaches. In the first model, following a previous work by Koch et al. [18], the respective contributions of homogeneous and inhomogeneous line broadening to the amplification and the saturation effects is explicitly taken into account. The second approach [19], aims at describing the effect of beam propagation in the different regions of the plasma. It is based on geometrical optics (ray tracing code) and takes into account the beam refraction due to density gradients, and the saturation effects. Refraction is known to limit the effective amplification length and leads to the beam travelling through plasma regions with various ion temperatures.

The evolution of the X-ray laser plasma, produced in conditions similar to those of the experiment, was simulated using the time-dependent 1.5D-Lagrangian hydrodynamic code EHYBRID [20]. Let us denote z the axis of the plasma rod, whereas the x-axis is the direction normal to the target surface (or parallel to the driving laser incoming direction). The y-axis is perpendicular to the z and the x-axis. EHYBRID describes in detail the hydrodynamic evolution of the plasma in the x-direction, whereas the transverse expansion is treated as self-similar. The fluid is divided into cells where Bremsstrahlung absorption of the laser pulse energy and its thermal diffusion into the plasma are taken into account. For the experimental intensity range, a thermal flux limiter of 0.1 was used, and the reflectivity at critical density was set to 0.7. Inside each cell, the ionisation is described by Griem's model [21]. In this model, the collisional recombination rate is given in terms of the collision limit, i.e., the lowest principal quantum number for which collisional excitation is as probable as radiative decay.

For the Ni-like Ag ionic stage, a detailed description is used, that involves 272 levels (all levels in the $n = 4$ and $n = 5$ manifolds and averaged contributions from $n = 6$

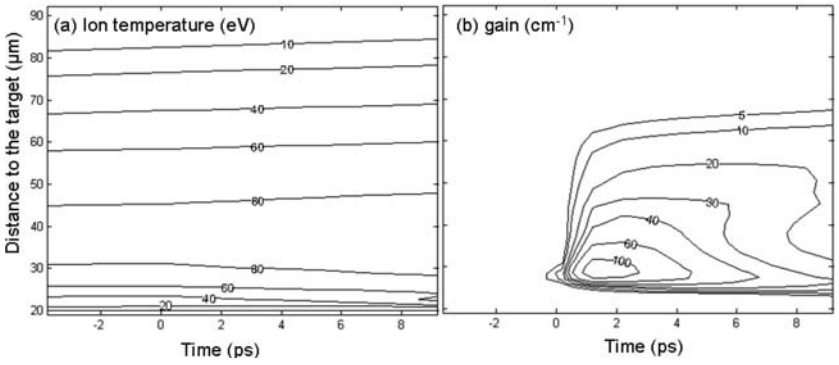

Fig. 4. Contours of ion temperature (a) and local gain (b) in the soft X-ray laser plasma as a function of time and distance to the target surface. The time of the short pulse peak irradiance is at 0 ps.

to $n = 8$). The level excitation and deexcitation rate coefficients were obtained by the HULLAC code [22] for all transitions between the $n = 4$ levels. For transitions involving higher levels, empirical formulae were used. Time and space variation of the spectrally-integrated spontaneous emission power $\sigma(x,t)$, small-signal gain $G_{SS}(x,t)$ and saturation intensity I_{sat} are deduced from the calculated level populations.

In Figure 4, calculated temporal and spatial evolutions of the plasma ion temperature (a) and local gain G_{ss} (b) are represented. The time $t = 0$ ps corresponds to the peak intensity of the short pulse, which occurs 250 ps later than the peak of the long pulse. One can see that the laser gain values (Fig. 4b) are significant during ∼10 ps in a region of the plasma located between 25 μm and 40 μm from the target surface. In this region and during the gain lifetime, the ion temperature is Ti ∼ 80 eV and the ion density is $\sim 9 \times 10^{19}$ cm^{-3}.

The predicted plasma parameters presented above are used as input data in the calculation of the X-ray laser line profile. Two different types of broadening effects contribute to the optically thin line profile $\Phi(\nu)$ of the lasing ions: the homogeneous and inhomogeneous effects. The finite lifetime of the lasing levels due to their natural decay and to electronic collisions, leads to a homogeneous broadening $\Delta\nu_L$ with a Lorentzian spectral profile ϕ:

$$\phi(\nu,\nu_0) = \frac{2}{\pi\Delta\nu_L}\frac{1}{1+\frac{4(\nu-\nu_0)^2}{(\Delta\nu_L)^2}}. \quad (1)$$

The homogeneous broadening is dominated by electronic collisions and its value is deduced from the electron temperature T_e and density n_e provided by the EHYBRID code. In the gain region, at the time of maximum gain, we have 300 eV $\leq T_e \leq$ 600 eV and 2×10^{20} cm^{-3} $\leq n_e \leq 5 \times 10^{20}$ cm^{-3} so that,the homogeneous linewidth is 2 mÅ $\leq \Delta\nu_L \leq$ 5 mÅ. The thermal motion of the ions causes an additional Doppler inhomogeneous broadening. To this mechanism is associated a Gaussian profile $S(\nu)$ of width $\Delta\nu_D$:

$$S(\nu,\nu_0) = \frac{1}{\Delta\nu_D}\left(\frac{4\ln 2}{\pi}\right)^{1/2}\exp\left(\frac{-4\ln 2(\nu-\nu_0)^2}{(\Delta\nu_D)^2}\right) \quad (2)$$

where $\Delta\nu_D = \nu_0\left(\frac{8kT_i\ln 2}{mc^2}\right)^{1/2}$. Here m is the ion mass and T_i. Since the ion density in the X-ray laser active region is lower than 10^{20} cm^{-3}, the Stark broadening produced by the slowly fluctuating plasma local field can be neglected. Finally Φ, the overall optically thin spectral profile of the spontaneous emission resulting from the homogeneous and inhomogeneous contributions, can be described by a Voigt profile:

$$\Phi(\nu) = \int_{-\infty}^{+\infty}\phi(\nu'-\nu)S(\nu')d\nu'. \quad (3)$$

The validity of this description has been checked by comparing the Voigt profile with the profile obtained by the line shape code PPP [23]. Finally the effect of frequency redistribution is neglected, hence the spontaneous emission and gain spectral profiles may be considered as identical.

In a first approach, we used a model described by Koch et al. [18], to calculate the spectral intensity profile of the soft X-ray laser line after amplification. This model is time independent and assumes a spatially uniform amplifying plasma. The evolution of the spectral intensity $I(\nu,z)$ with the amplifying length z is calculated by numerically integrating the following differential equation:

$$\frac{dI(\nu,z)}{dz} = \frac{\sigma(\nu_0)}{\Phi(\nu_0)}\left(1+\frac{G_{SS}I(\nu,z)}{\sigma(\nu_0)}\right) \times \int_0^{\infty}\frac{S(u)\phi(\nu,u)du}{1+\frac{1}{I_{sat}}\int I(\nu',z)\phi(\nu',u)d\nu'} \quad (4)$$

with the notations previously defined. The full width at half maximum resulting from this calculation has been plotted as a function of the amplifying length in Figure 5. The ratio of saturation intensity versus spontaneous emission was set to reproduce the gain saturation ($G = G_{ss}/2$) for $G_{ss}L = 12$.

It was checked that the results shown in Figure 5 depend weakly on the value of $G_{ss}L$ at which saturation occurs. The calculations were made for two different values of homogeneous broadening ($\Delta\nu_L = 5$ mÅ and 1 mÅ), consistent with the range of plasma parameters predicted by our hydrocode. For the two different ionic temperatures considered (kT_i = 80 eV and 10 eV), the corresponding inhomogeneous linewidths ($\Delta\nu_D$ = 9 mÅ and 1 mÅ) are found to be larger than or of the same order of magnitude that the homogeneous contributions. The overall optically thin linewidth $\Delta\nu_0$ is given by the line

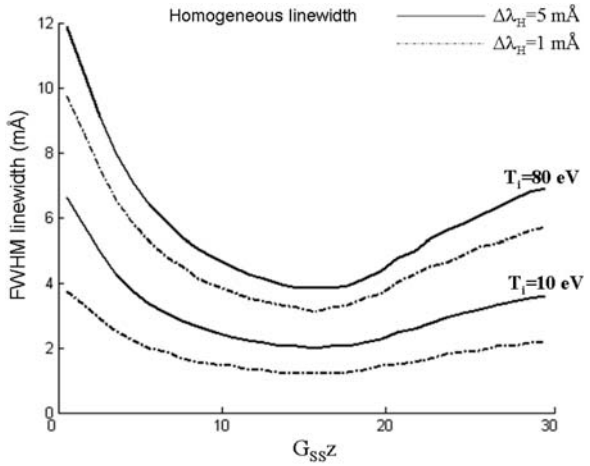

Fig. 5. Calculated dependence of the soft X-ray laser line width (FWHM) with amplification length for different ion temperatures (10 eV and 80 eV) and homogeneous linewidths. Saturation is assumed to be reached for a gain length of 12.

width at $G_{ss}L = 0$ (no amplification). For the small values of the gain-length product corresponding to the small-signal regime the X-ray laser line width rapidly decreases with the amplification length with a scaling law given by $\Delta\nu(L) = \Delta\nu_0/(G_{SS}L)^{1/2}$. This evolution ends when the intensity reaches values of the order of magnitude of the saturation intensity I_{sat} where the linewidth reaches a minimum and then slowly rebroadens. For an ion temperature of $T_i = 80$ eV, consistent with the predictions of EHYBRID, the minimum linewidth achieved is between 3.2 mÅ and 3.9 mÅ, depending on the homogeneous width $\Delta\nu_L$. To achieve a linewidth smaller than 1 mÅ, closer to the experimental value, a very strong gain narrowing would be required corresponding to a completely unrealistic gain-length product of 100, greater than the saturation gain length product. On the other hand the lower curve of Figure 5 shows that the experimental value could also be achieved with our calculations by considering a very low ion temperature, lower than 10 eV. This is in contradiction with predictions of the hydrocode.

This first modelling approach does not take into account the gradient of electron density existing in the direction of plasma expansion and hence the refraction of the amplified beam in the corresponding gradient of refraction index. This effect is known to play an important role in the limitation of the amplification and was included in the second approach that was used to calculate the X-ray laser spectral profile. This second model is based on a ray-tracing post processor to the EHYBRID code. It was developed by Kuba et al. [24], to perform simulation of the beam propagation and amplification.The evolution of the spectral intensity profiles is calculated along the trajectories of more than one million rays launched with different initial coordinates and initial angles, at the beginning of the plasma and at the time of the peak gain predicted by EHYBRID. Rays trajectories depends on the electron density gradient $\nabla n_e(\mathbf{r}, t)$ and are fully described by the eikonal equation:

$$\frac{d}{ds}\left(n\frac{d}{ds}\mathbf{r}\right) = \nabla n(\mathbf{r}, t) \tag{5}$$

where n is the refractive index of the plasma ($n = \sqrt{1 - n_e(\mathbf{r})/n_c}$), $\mathbf{r}$ the position vector, ds the differential ray path element and n_C is the critical electron density at the soft X-ray laser wavelength. The electron density, as calculated by EHYBRID, is a function of the coordinates $\mathbf{r}$ and t. The small signal gain, emissivity, electron density, electron and ion temperatures along the ray trajectory are read from data files provided by EHYBRID. To take the temporal evolution of the plasma into account, the data are updated every 0.1 ps. The beam propagation is dominated by the strong refraction effect that occurs in the x-direction. Without any lack of generality, ray tracing calculations have been performed only in the median plan of the expanding plasma ($y = 0$).

The evolution of the spectral intensity of the X-ray laser along a ray is calculated by the following relation that describes the small signal regime as well as the saturation regime:

$$I(\nu, s, t) = \frac{\sigma(\nu, x, t)}{G(\nu, x, t)}\left[e^{G\Delta s} - 1\right] + I(\nu, s - \Delta s, t)e^{G\Delta s} \tag{6}$$

where Δs is a small discrete interval along the ray path, and $G = G(\nu, x, t)$ is the saturated gain. Assuming an optically thin profile dominated by the inhomogeneous Doppler broadening, G depends on the spectral intensity $I(\nu, s, t)$ as follows:

$$G(\nu, x, t) \approx \frac{G_{SS}(\nu, x, t)}{1 + \frac{I(\nu, x, t)}{I_{sat}}}. \tag{7}$$

In equation (5) and (6), the spectral profile is involved in the spontaneous emission power σ and in the small signal gain G_{SS} as follows:

$$\sigma(\nu, x, t) = N_u h\nu\frac{\delta\Omega}{4\pi}A_{ul}\Phi(\nu, x, t) = \sigma(0, x, t)\Phi(\nu, x, t) \tag{8}$$

$$G_{SS}(\nu, x, t) = h\nu\frac{B_{ul}}{c}\left[N_u(x, t) - \frac{g_u}{g_l}N_l(x, t)\right]\Phi(\nu, x, t). \tag{9}$$

Here, $\delta\Omega$ is the solid angle of the spontaneous emission contributing to the power carried by the ray, A_{ul} and B_{ul} are the Einstein coefficients for spontaneous and stimulated emissions between the upper (u) and lower (l) lasing levels, of population N_u and N_l and of statistical weights g_u and g_l.

The optically thin spontaneous emission spectral profile is assumed to be a Voigt profile. Figure 6a presents the intensity profile $I(\lambda)$ calculated for the rays that experience the highest amplification and give the major contribution to the peak output power. Two amplification lengths are represented, $L = 0.2$ mm (Fig. 6a) and

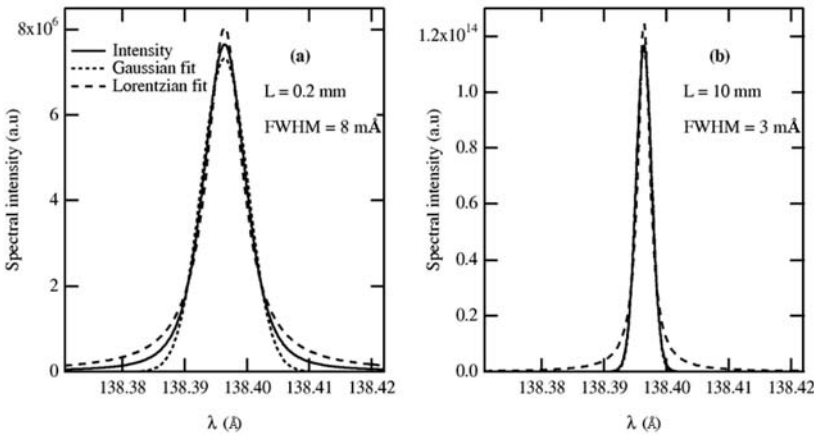

Fig. 6. Calculated soft X-ray line profile resulting from a ray-tracing simulation. (a) After an amplification in 0.2 mm of plasma, and (b) 10 mm. Profiles are compared to Lorentzian and Gaussian fitted profiles.

$L = 10$ mm (Fig. 6b). The overall optically thin linewidth in the absence of amplification was equal to 12 mÅ. For $L = 0.2$ mm, the linewidth is already reduced to 8 mÅ. A curve fitting of $I(\lambda)$ indicates clearly that at this stage the amplified profile is neither Doppler nor Lorentzian. After $L = 10$ mm in the plasma, the linewidth is reduced to 3 mÅ, and the profile $I(\lambda)$ is clearly Gaussian. The calculated value of 3 mÅ is thus larger than the experimental linewidth but is in agreement with the minimum value predicted by the first model presented above, for the ionic temperature of 80 eV. Using the Wiener-Khintchine theorem, we find that the calculated linewidth corresponds to a coherence time and a coherence length that are respectively $\tau_C = 1.1$ ps and $\ell_C = 340$ μm.

In conclusion, the two modelling approaches presented above yield similar values for the X-ray laser spectral line widths. The calculated values are more than three times greater than the width deduced from experimental results. In the next section we will discuss possible reasons that could explain this discrepancy.

4 Discussion

A first possible reason for the above discrepancy may involve other effects such as Dicke narrowing [25], not considered in our simulations. This effect, which leads to a narrower initial Doppler profile, is expected to occur when the lasing ion mean free path λ_{ii} is shorter than the X-ray laser wavelength: $\lambda > \lambda_{ii}$.

This effect was first discussed by Griem [26] in the context of X-ray lasers. An order of magnitude of λ_{ii} can be obtained from Spitzer theory [27], using plasma parameters given by the hydrodynamic simulation: $\lambda_{ii} = 0.25$ nm. This value is hence smaller than the X-ray laser wavelength and this could be an argument to further investigate the influence of the Dicke narrowing in the X-ray laser line profile.

However later work by Pollock and London [28] has shown that for the relatively large coupling factors Γ relevant to X-ray laser plasmas, the criterion using λ_{ii} from Spitzer theory is not valid and more refined calculations, involving molecular dynamics, are required. For the plasma conditions relevant to the transient X-ray laser considered here, the ion coupling factor is $\Gamma \sim 3$. In this case the effect of ion collisional narrowing of the Doppler profile, or Dicke narrowing, is not negligible but still much too low to account for the observed discrepancy between experiment and simulation.

We have investigated another possible reason for the observed discrepancy between measurements and numerical predictions. It involves the temporal and statistical behaviour of the TCE X-ray laser field $E(t)$. In Section 2 the spectral line width was inferred from the fringe visibility by using the Wiener Khintchine theorem. This theorem is valid if the field $E(t)$ is stochastic, but it also assumes that the field is stationary and ergodic. The same hypotheses are also implied in the calculations presented in Section 3, which rely on a radiative transfer description of the amplification of the field intensity. However in our experiment we have shown that the duration of 6 ps measured for the X-ray laser pulse is only a few times longer than the coherence time τ_C. This means that the electromagnetic field $E(t)$ associated to the X-ray laser signal is far from being stationary. A better description of $E(t)$ can be adapted from the work developed by Lajunen et al. [29] in the context of diode lasers. Following this work we model the X-ray laser field by a stationary, ergodic random field, temporally modulated by a Gaussian shape envelop, which accounts for the finite duration of the pulse. Using the formalism described in [29] we find that the coherence length of the modulated field is slightly smaller than what would be obtained by considering the stationary part of the field alone. Hence if the finite-duration correction was introduced in the stationary-field calculations described in Section 3, this would lead to a slightly smaller coherence length and an increased discrepancy with the experimental results.

Finally, we propose an alternative explanation that involves the statistical fluctuations of the X-ray laser field and the definition of the coherence degree. All the experimentally accessible quantities such as density of spectral power, degree of coherence or fringe visibility involve a statistical average over all the possible realisations of $E(t)$, because the field structure is fluctuating from one realisation to another, due to its stochastic nature. In the case of a stationary field this statistical average can be replaced

by an average over time, for example through integration by the detector. However, in our experiment the time-integrated interferogram obtained in a single shot does only include a small number of field realisations, since the X-ray laser pulse is composed of a small number of wave trains. We thus expect the fringe visibility inferred from interferograms to fluctuate from shot to shot. In that case the temporal average should be replaced by a statistical average over a large number of shots, performed in identical conditions. In our experiment however the limited number of shots available in the experimental campaign did not allow to have more than three interferograms for each path difference. The average visibility (Fig. 3) inferred from such a limited data set may not properly account for the shot-to-shot fluctuations inherent to the measurement. A preliminary investigation of this effect shows that the amplitude of the fluctuations increases with the path difference, while the visibility cannot be less than zero. This would lead to an overestimation of the visibility for the larger path difference and hence to an over estimation of the coherence length. The detailed investigation of this effect is however beyond the scope of this paper and is left for future work.

5 Conclusion

We have inferred the spectral shape and width of the TCE Ni-like silver X-ray laser from the experimental measurement of its longitudinal coherence. The 13.9 nm line exhibits a Lorentzian profile with a FWHM of 0.73 mÅ. This is to our knowledge the narrowest spectral width ever measured for an X-ray laser or for any source in that spectral range. We have performed numerical simulations of the amplified line profile along two different approaches. Both approaches lead to a predicted linewidth that is 3 times larger than the measured value. We discuss different effects which might explain this discrepancy. We show that, in our particular case where the coherence time is of the same order of magnitude as the pulse duration, the field associated to the X-ray laser signal cannot be considered as stationary. We suggest that shot-to-shot fluctuations inherent to the measurement of the visibility could have led to an overestimation of the coherence length. Further detailed investigations of this effect are underway and will be presented in another paper.

The financial support of the L.E.A. (Laboratoire Europeen Associé) is gratefully acknowledged. This work was also partially supported by an A.C.I. Photonique grant. We would like to thank the technical staff at LULI for their support in conducting the experiment at LULI. We are indebted to G.J. Pert (University of York, UK) for providing the code EHYBRID.

References

1. H. Daido, Rep. Prog. Phys. **65**, 1513 (2002)
2. D.L Matthews, P.L. Hagelstein, M.D. Rosen, M.J. Eckart, N.M. Ceglio, A.U. Hazi, H. Medecki, B.J. Macgowan, J.E. Trebes, B.L. Whitten, E.M. Campbell, C.W. Hatcher, A.M. Hawryluk, R.L. Kauffman, L.D. Pleasance, G. Rambach, J.H. Scofield, G. Stone, A. Weaver, Phys. Rev. Lett. **54**, 110 (1985)
3. J.J. Rocca, V. Shlyaptsev, F.G. Tomasel, O.D. Cortazar, D. Harthorn, J.L.A. Chilla, Phys. Rev. Lett. **73**, 2192 (1994)
4. P.V. Nickles, V.N. Shliaptsev, M. Kalachnikov, M. Schnurer, I. Will, W. Sander, Phys. Rev. Lett. **78**, 2748 (1997)
5. R. Keenan, J. Dunn, V.N. Shlyaptsev, R.F. Smith, P.K. Patel, D.F. Price, Proc. SPIE **5197**, 117 (2003)
6. P.V. Nickles, K. Janulewicz, G. Priebe, A. Luciatti, R.K. Kroemer, A.K. Gerlitz, W. Sandner, Proc. SPIE **5197**, 29 (2003)
7. Y. Abou-Ali, A. Demir, G.J. Tallents, M. Edwards, R.E. King, G.J. Pert, J. Phys. B **36**, 4097 (2003)
8. J.C. Chanteloup, E. Salmon, C. Sauteret, A. Migus, P. Zeitoun, A. Klisnick, A. Carillon, S. Hubert, D. Ros, P. Nickles, M. Kalashnikov, J. Opt. Soc. Am. B. **17**, 151 (2000)
9. Y.Abou-Ali, G.J. Tallents, M. Edwards, R.E. King, G.J. Pert, S.J. Pestehe, F. Strati, R. Keenan, C.L.S. Lewis, S. Topping, O. Guilbaud, A. Klisnick, D. Ros, R. Clarke, D. Neely, M. Notley, A. Demir, Opt. Comm. **215**, 397 (2003)
10. A. Klisnick, J. Kuba, D. Ros, R. Smith, G. Jamelot, C. Chesnais-Popovics, R. Keenan, S.J. Topping, C.L.S. Lewis, F. Strati, G.J. Tallents, D. Neely, R. Clarke, J. Collier, A.G. Macphee, F. Bortolotto, P.V. Nickles, K.A. Janulewicz, Phys. Rev. A. **65**, 33810 (2002)
11. A. Klisnick, O. Guilbaud, D. Ros, K. Cassou, S. Kazamias, G. Jamelot, J.-C. Lagron, D. Joyeux, D. Phalippou, Y. Lechantre, M. Edwards, P. Mistry, G.J. Tallents, J.Q.S.R.T. **99**, 370 (2006)
12. R.F. Smith, J. Dunn, J. Nilsen, J.R. Hunter, S. Hubert, S. Jacquemot, C. Raimond, R. Marmoret, M. Fajardo, Ph. Zeitoun, L. Vanbostal, C.L.S. Lewis, M.F. Ravet, F. Delmotte, Opt. Lett. **28**, 1 (2003)
13. I.N. Ross et al., Appl. Opt. **26**, 1584 (1987)
14. O. Guilbaud et al., Proc. SPIE **5197**, 17 (2003)
15. D. Joyeux, R. Mercier, D. Phalippou, M. Mullot, M. Lamare, *Proceedings of the 7th international conference on X-ray lasers* (EDP Sciences, Paris, 2000), p. 511
16. H. Tang et al., Jpn. J. Appl. Phys. **48**, 443 (2003)
17. M. Born, E. Wolf, *Principles of Optics*, 7th edn. (Cambridge University Press, 1999)
18. J.A. Koch, B.J. Macgowan, L.B. Dasilva, D.L. Matthews, J.H. Underwood, P.J. Batson, R.W. Lee, R.A. London, S. Mrowka, Phys. Rev. A. **50**, 1877 (1994)
19. D. Benredjem et al., J.Q.S.R.T. **99**, 67 (2006)
20. G.J. Pert, J. Fluid. Mech. **131**, 401 (1983)
21. H.R. Griem, *Plasma spectroscopy* (Mc Graw-Hill, New York, 1964) p. 241
22. A. Bar-Shalom, M. Klapisch, J. Oreg, J.Q.S.R.T. **71**, 169 (2001)
23. B. Talin, A. Calisti, L. Godbert, R. Stamm, R.W. Lee, L. Klein, Phys. Rev. A **51**, 1918 (1995)
24. J. Kuba, D. Benredjem, C. Möller, L. Drska, J. Opt. Soc. Am. B **20**, 609 (2003)
25. R.H. Dicke, Phys. Rev. **89**, 472 (1953)
26. H.R. Griem, Phys. Rev. A **33**, 3580 (1986)
27. L. Spitzer, R. Harm, Phys. Rev. **89**, 977 (1953)
28. F. Pollock, R. London, Phys. Fluids **B5**, 4495 (1993)
29. H. Lajunen, J. Tervo, J. Turunen, P. Vahimaa, F. Wyrowski, Opt. Expr. **11**, 1894 (2003)